Journal of Ultrafine Grained and Nanostructured Materials
https://jufgnsm.ut.ac.ir
Vol. 55, No.2, December 2022, pp. 122-132
Print ISSN: 2423-6845 Online ISSN: 2423-6837
DOI: 10.22059/jufgnsm.2022.02.04

Ni-Al_2O_3 Nanocomposite with High Specific Surface Area Synthesized by Mixture of Fuels through Solution Combustion

H. Nasiri[,1], J. Vahdati Khaki[2], N. Shahtahmassebi[3]*

[1]Department of Materials Engineering, Faculty of Mechanic and Materials Engineering, Birjand University of Technology, Birjand, Iran;
[2]Department of Materials Science and Engineering, Engineering Faculty, Ferdowsi University of Mashhad, Mashhad, Iran;
[3]Department of Physics, Faculty of Sciences, Ferdowsi University of Mashhad, Mashhad, Iran.

Recieved: 15 December 2021; Accepted: 17 January 2022

**Corresponding author email: nasiri@birjandut.ac.ir*

ABSTRACT

This paper investigates the application of a mixture of three types of fuels, namely urea, glycine and hydrazine, for the synthesis of Ni-10 wt. % Al_2O_3 nanocomposite using the solution combustion method. Nickel and aluminum nitrates are used as an oxidizer. The fuels are used at two different fuel to oxidizer ratios. DSC-TGA diagrams prove hydrazine-nitrate reaction system can ignite before nitrate decomposition in contrary to urea-nitrate and glycine-nitrate systems. The results showed synthesized alumina at combustion temperatures less than 500 ºC is amorphous and the combustion temperatures more than 600 ºC made alumina crystalline. The measured surface area for the synthesized nanocomposite in air and less than 10 min was 207 $m^2 g^{-1}$. SEM and FESEM images prove the presence of small porosities in the synthesized nanocomposites. TEM image shows synthesized alumina in the nanocomposite has a mean particle size of less than 25 nm.

Keywords: *Nickel, Alumina, Combustion, Nanocomposite, Urea, Hydrazine.*

1. Introduction

Nowadays, materials with ultra-fine grain size and high specific surface area have found a special place in academia as well as industry. Compared to other novel methods of fabricating high surface materials and composites, solution combustion synthesis (SCS) has interesting features [1,2]. As a type of self-propagation high-temperature synthesis (SHS) process, SCS is more attractive than SHS for the same synthesis products produced by two methods. This is because, compared to the SHS, the SCS requires lower initial thermal energy and it can produce higher quality powders. Other attractive characteristics of the SCS method pertain to its fast and simple process and its ability to synthesize versatile material with acceptable levels of homogeneity [3, 4]. Also, the high volume of gases generated during the combustion significantly prevents the sintering of the particles to each other [5, 6].

In-situ oxidation-reduction reactions of metal salts and fuels in SCS can produce a crystalline structure as the final product without requiring an external heat source in short times [7,8]. Thus, there is no need for the subsequent high temperature processing of the products. This prevents unwanted grain growth [9]. Some of the main factors affecting the synthesized products are: fuel type, fuel to oxidizer ratio (F/O), a mixture of fuels, heating rate, and atmosphere of the combustion reaction [2, 10]. By controlling the exothermicity and intensity of the reaction, fuel can play an important

role in the synthesis mode of the reaction [11]. It can determine whether the reaction takes place in spontaneous flaming or smoldering modes. Such different modes can result in the production of different types of powder even with the same initial raw materials [12]. The mixture of fuels effects on synthesis conditions was studied by different research groups. Investigations revealed using two or three fuels simultaneously can cause special conditions and properties. In some reactions one fuel is not able to prepare a suitable synthesis as required. The drawbacks can be amorphous synthesized materials, low surface area and even synthesis cannot occur, but a mixture of fuels can cover disadvantages of each fuel than when uses individually [13-16].

Ni-Al_2O_3 nanocomposite has many applications as catalytic and solar cell materials [17, 18]. The catalytic aspect of this nanocomposite is highly regarded. The researchers try to increases the catalytic potential of nickel and its oxides by different methods such as: increasing surface area or using different support materials [19, 20]. One of the most favorable catalyst support materials is alumina because of its high surface area. Among all transition alumina structures γ-Al_2O_3 is more favorable [21, 22].

As mentioned, in order to increase the efficiency and improve the properties of this nanocomposite, it is essential to achieve powders with a high specific surface area. Although it is possible to synthesize materials through SCS just with one type of fuel, a mixture of several types of fuels with different exothermicity can help achieve a higher specific surface area [23].

In order to synthesize Ni-Al_2O_3 nanocomposite with a high specific surface area, this research is devoted to investigating the effect of a mixture of three types of fuels with different reaction behaviors. It helps have advantages of all fuels simultaneously. Another objective pursued in this research is to achieve the maximum possible surface area by eliminating the reduction step and only using the combustion step to synthesis the nanocomposite. As a result, the final nanocomposite can be synthesized with a high surface area (207 m^2g^{-1}) in the air in less than ten minutes.

2. Experimental

2.1. Materials and methods

In this study, the following reactant materials are used as the oxidizer in the solution: (1) nickel nitrate, $Ni(NO_3)_2.6H_2O$ (≥99% - Merck), and (2) aluminum nitrate, $Al(NO_3)_3.9H_2O$ (≥99%- JHD). The three types of fuels used in the SCS method include Urea (≥98.5%- Panreac), hydrazine hydrate (80%- Scharlau) and glycine (≥99%). Also, graphite is used as an auxiliary material. Equations 1 to 3 are set to have Ni-10wt. %Al_2O_3 for urea, glycine and hydrazine reaction systems, respectively. According to the equations below, the exact amount of alumina is 10 wt. % in urea and hydrazine systems and 9.9wt. % in the glycine system.

$$12.5Ni(NO_3)_2 + 1.6Al(NO_3)_3 + 29CO(NH_2)_2 \rightarrow 12.5Ni + 0.8Al_2O_3 + 29CO_2 + 58H_2O + 43.9N_2 \quad (1)$$

$$12.66Ni(NO_3)_2 + 1.6Al(NO_3)_3 + 19.55C_2H_5NO_2 \rightarrow 12.66Ni + 0.8Al_2O_3 + 39.1CO_2 + 48.86H_2O + 24.8N_2 \quad (2)$$

$$12.45Ni(NO_3)_2 + 1.6Al(NO_3)_3 + 43.35N_2H_4 \rightarrow 12.45Ni + 0.8Al_2O_3 + 86.7H_2O + 58.2\ N_2 \quad (3)$$

The amount of graphite used is calculated to prevent the oxidation of nickel. If the initial amount of nickel nitrate is 3 g, the final metallic nickel, i.e., after synthesis and complete reduction, amounts to 0.6 g. According to Equation 4, this amount of nickel can be oxidized to NiO by 0.005 mol of oxygen. In turn, the amount of graphite, which is determined based on the amount of oxygen, is calculated to be about 0.12g (Equation 5).

$$Ni + 1/2O_2 = NiO \quad (4)$$

$$C + 1/2O_2 = CO \quad (5)$$

In order to manage the scope of the experiments, the fuel to oxidizer (F/O) (weight ratio) is fixed and limited to two levels, i.e., 1 and 1.5, for all fuels. The solution includes the mixture of all three types of fuels associated with nickel and aluminum nitrates.

An alumina cap is used as a container. A hot plate, preheated to 330 °C, is used as a means to heat the reactants to their respective ignition temperatures. All synthesis reactions are carried out in the air.

2.2. Materials Characterization

A Philips X'pert diffractometer is used with Cu K_α radiation of 0.15406 nm in the range of 2θ = 4–80° by the step of 0.02° for X-ray diffraction (XRD) analysis. Microscopic evaluations are carried out using an LEO VP 1450 scanning electron microscope (SEM), a Mira 3-XMU

field emission SEM (FESEM) and a Philips Tecnai F20 FEG-STEM transmission electron microscopy (TEM). The specific surface area is measured by a BET (Brunauer–Emmett–Teller) Sorptometer-210-A (N_2 adsorption at -195°C). Before BET measurements, all samples are kept at 100°C for 3h to remove moisture on the surface of the samples. A SETARAM instrument (SETYS Evolution-1750) differential scanning calorimetry (DSC) is used for calorimetric analyses. The ignition and combustion temperatures are measured by an Advantech USB4718 data acquisition unit and K type thermocouple. This device is capable of transferring temperature data from the reaction environment to the computer at a frequency of 10 hertz. The mean accuracy of measurements is about ±3°C and ±20°C for ignition and combustion temperatures, respectively.

3. Results and discussion

In the first place, the thermal decomposition behavior of the raw materials is studied. DSC-TGA diagrams of nickel and aluminum nitrates are shown in Fig 1a and 1b.

It can be seen the first endothermic peaks for nickel nitrate (71°C) and aluminum nitrate (108°C) belong to the melting points of nitrates, because the TGA diagram did not show weight decrease. The endothermic decomposition peaks for nickel nitrate were recorded at 149°C, 175°C, 202°C and 322°C, respectively. Aluminum nitrate revealed only one endothermic decomposition peak close to 150 °C. Fig 2a to 2c show the DSC-TGA diagrams for urea, glycine, and hydrazine, respectively.

Fig 2a shows the first endothermic peak (131°C) for urea belongs to the urea melting point. The decomposition of urea starts at 220°C and for glycine and hydrazine (Fig 2b and 2c) the endothermic peaks started at 250°C and 105°C, respectively. Also, in order to further shed light on this matter, the reactions of each fuel type with nickel and aluminum nitrates were studied and the results are presented in Table 1. The time of reaction is the time spends between the ignition

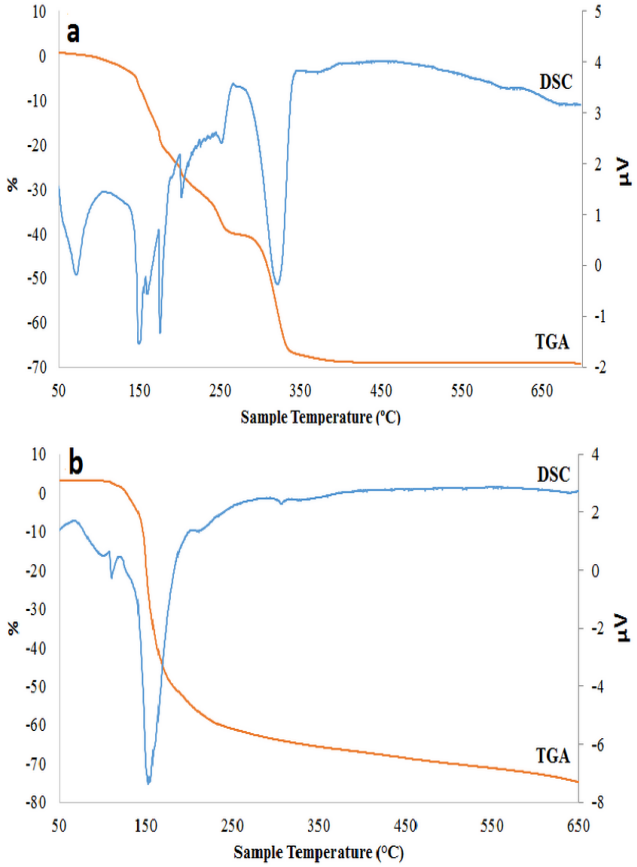

Fig. 1- DSC-TGA diagrams for a: $Ni(NO_3)_2.6H_2O$ and b: $Al(NO_3)_3.9H_2O$ in air, heating rate 10 °C min^{-1}.

Table 1- Data for each fuel type when individually reacting with nitrates

fuel	F/O	Ignition temperature (°C)	combustion temperature (°C)	time of reaction (s)
urea	1	314	429	3.9
glycine	1	270	574	1.7
hydrazine	1	110	246	0.4
urea	1.5	288	730	3.1
glycine	1.5	286	443	10.8
hydrazine	1.5	114	665	2.9

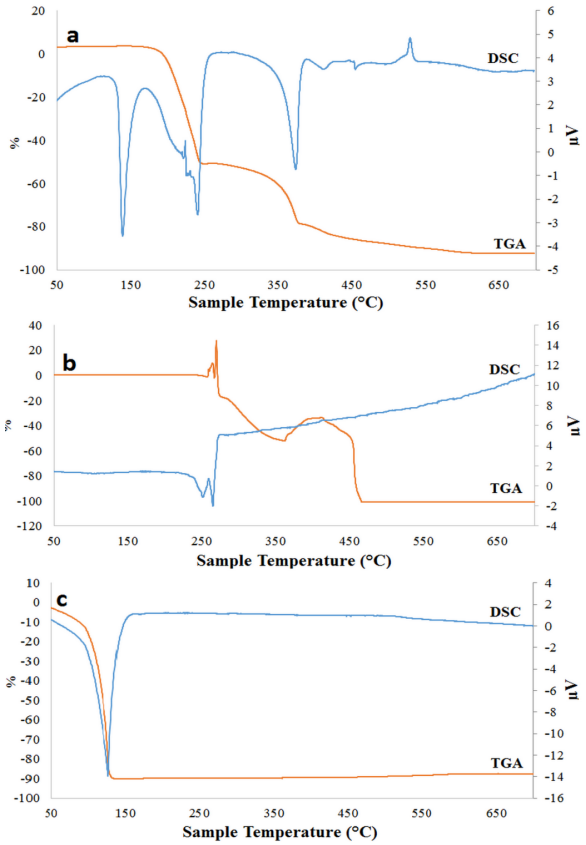

Fig. 2- DSC-TGA diagrams for a: urea, b: glycine and c: hydrazine in air, heating rate 10 °C min^{-1}.

and combustion temperatures.

In Table 1 the ignition temperatures are 110°C and 114°C for hydrazine at F/O ratios 1 and 1.5, respectively. According to Fig 1, those ignition temperatures are below the nitrates decomposition temperatures. The ignition temperatures of the nitrate-hydrazine system are in accordance with the hydrazine boiling temperature (Fig 2c). It shows when uses hydrazine as fuel, combustion synthesis can occur even before nitrates decomposition. It is because, after boiling the temperature of hydrazine, produced gases prefer to react with the oxygen of the air [24]. So, a higher amount of hydrazine in the reaction can increase the combustion temperature. Such behavior can be seen in Table 1.

In Table 1 the ignition temperatures for urea at F/O ratios 1 and 1.5 are 314°C and 288°C, and for glycine are 270°C and 286°C, respectively. By comparison with decomposition temperatures of nitrates in Fig 1, it can be seen the combustion synthesis for urea and glycine can occur when nitrates and fuels decompose. In other words, the source of energy for carrying out the combustion synthesis is oxidation-reduction reactions that occur between decomposed nitrates and fuels (urea and glycine). As a result, the maximum temperature for nitrate-urea and nitrate-glycine systems should be at F/O=1[24, 25]. So, the additional amounts of these fuels (greater than stoichiometric ratio) can decrease the combustion temperature that

called diluent role, because decomposition of urea and glycine is endothermic and takes the heat of combustion synthesis.

The mentioned behavior can be seen for glycine. In Table 1 the combustion temperature decreased by 131°C when the F/O ratio increased. The decrease of combustion temperature can make synthesis unstable, as shown in Fig 3.

It can be seen in Fig 3, the transition from the ignition to combustion temperatures occurred very rapidly for urea and hydrazine. Nevertheless, glycine did not show a stable reaction and the time of reaction, was too long, i.e., 10.8 s. The mentioned time was calculated from ignition temperature to combustion temperature, and not for all range of the peak.

In the Table 1, urea showed an increase in its combustion temperature when the corresponding F/O ratio increased. The increase in the combustion temperature which occurs when the amount of urea is increased can be attributed to the fact that the decomposition of urea starts at a temperature much less than nitrate-urea system ignition temperature. Such difference can lead to the waste of urea before the combustion reaction, which in turn translates into a lowered amount of available urea at the reaction time. In other words, although the theoretical amount of urea, which is required for the combustion to occur with a maximum temperature, is at F/O=1, the necessary amount in the practical experiment is greater than F/O=1.

To support this argument, the combustion temperatures for different F/O ratios of 1, 1.1, 1.2, 1.3, 1.4 and 1.5 for urea and hydrazine are plotted in Fig 4.

According to Fig 4, the combustion temperature for urea first increases, from F/O of 1 to 1.3, and then decreases, for F/O of 1.4 and 1.5. This means that in the experiment conditions, F/O about 1.3 acts similar to the theoretical stoichiometric ratio, i.e., F/O=1. After F/O=1.3 any excessive urea can act as a diluent and decrease the combustion temperature as expected. According to Fig 2a and Table 1, the differences between the beginning decomposition temperature of urea (220°C) and ignition temperatures are about 68°C and 94°C for F/O ratios 1 and 1.5, respectively. Also, TGA of urea shows such difference can waste about 30wt. % of urea before reaction. As a result, first, urea should compensate its weight loss that occurs before reaction then more amounts of urea act as a diluent and decrease the combustion temperature.

For glycine, the differences between decomposition temperature and the ignition temperatures according to Fig 2b and Table 1 are about 22°C and 36°C, and such differences can cause the decrease of glycine about 4wt. % before combustion reaction. In Fig 4 the combustion temperature for hydrazine constantly rises with the increase in F/O as expected.

The details of experiments in the presence of three fuels are summarized in Table 2. As shown in this Table, all eight sample groups have a mixture of three fuels, but with different ratios. The two-factorial statistical method is used to determine the optimum number and order of mixtures needed for the experiment [26].

Table 2 suggests a wide range of combustion temperatures from 470°C to 739°C, such difference can be referred to both content of fuels and F/O ratios in each mixture. The lowest combustion temperature belongs to synthesis 1 that the content

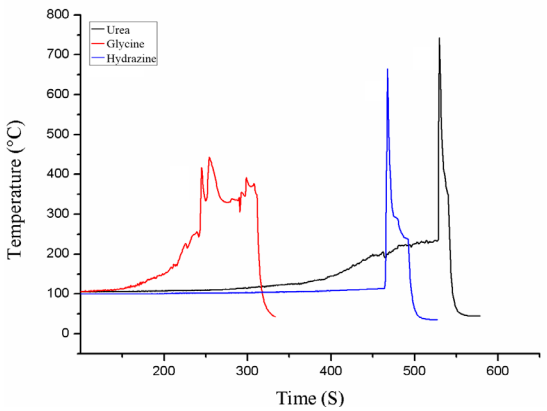

Fig. 3- Time-Temperature diagrams for different fuel reaction systems with F/O=1.5.

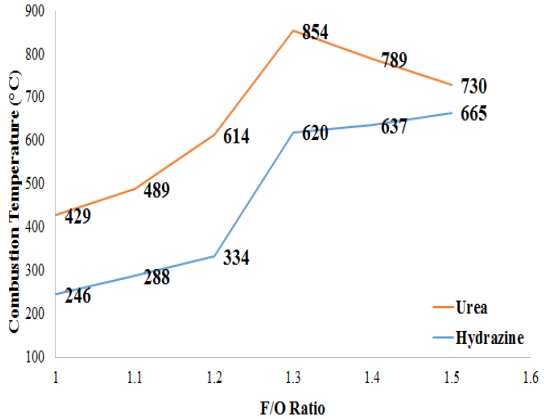

Fig. 4- Combustion temperatures for urea and hydrazine with F/O ratios of 1, 1.1, 1.2, 1.3, 1.4, and 1.5.

Table 2- Three-fuel mixture at two levels of F/O

synthesis number	fuel to oxidizer ratio for urea	fuel to oxidizer ratio for glycine	fuel to oxidizer ratio for hydrazine	combustion temperature (°C)
1	1	1	1	470
2	1.5	1	1	671
3	1	1.5	1	584
4	1.5	1.5	1	623
5	1	1	1.5	638
6	1.5	1	1.5	739
7	1	1.5	1.5	726
8	1.5	1.5	1.5	664

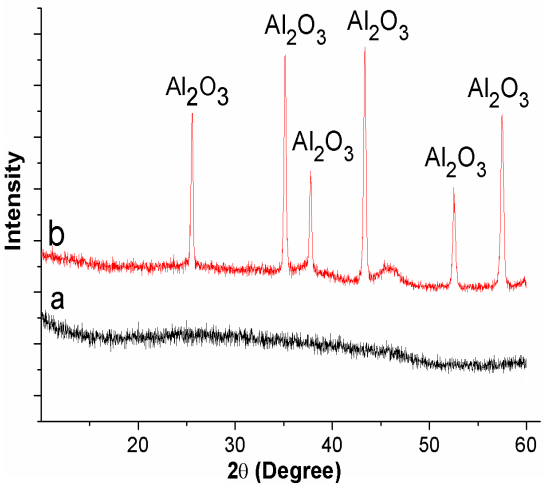

Fig. 5- XRD patterns for residual of synthesized nanocomposite (number 1) after solving in nitric acid, a: without calcination, b: after calcination at 900ºC for 1 h.

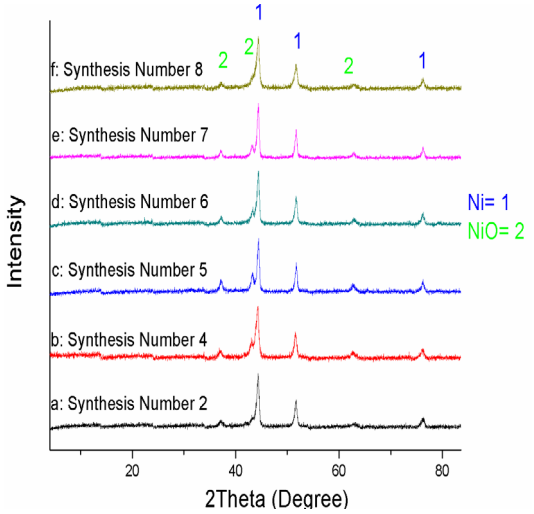

Fig. 6- The XRD results for six synthesized powders presented in Table 2.

of fuels and F/O ratios are the lowest. The highest temperatures are for numbers 6 and 7, respectively. It is because hydrazine is at its high level and one of urea or glycine is at a low level. As mentioned above, contrary to urea and glycine, higher content of hydrazine increases the combustion temperature. It can be seen in synthesis 8 when all fuels are at F/O=1.5 the combustion temperature was decreased because of the diluent role of additional urea and glycine.

One of the main reasons for choosing SCS is to fabricate both nickel and alumina as crystalline. Alumina must reach temperatures greater than 500-600 °C to avoid amorphous synthesis. So, the synthesized nanocomposite for synthesis number 1 was solved in nitric acid (5 M) and the residual was sent for XRD analysis. The result of XRD is presented in Fig 5.

As it can be seen in Fig 5a, the residual shows an amorphous phase. So, the residual was calcined at 900 °C for 1h. The XRD analysis was carried out again and the result illustrates in Fig 5b. It revealed the amorphous material was alumina. As a result, between mixtures presented in Table 2, only those with a combustion temperature greater than 600 °C were analyzed with XRD, i.e., mixtures 2, 4, 5, 6, 7, and 8. The results of the XRD analysis are shown in Fig 6.

Fig 6 shows that even though the mixtures of three types of fuels were used, none of the six mixtures studied were able to synthesize the Ni-Al_2O_3 nanocomposite as a final product. In all XRD patterns, a combination of Ni and NiO was observed.

Two methods can be applied to eliminate the nickel oxide phase. The first method is to use a reduction atmosphere (like H_2) after the synthesis step. In addition to being time-consuming, using a reductive atmosphere can result in the reduction of the specific surface area because of unwanted grain growth or sintering [27].

The second method is to prevent nickel oxidation in the air after synthesis. As a result, to prevent the metallic nickel oxidation was inhibited

by using an auxiliary material, namely graphite. At temperatures greater than 435°C, graphite is more prone to oxidation than metallic nickel [28]. Also, the rate of graphite oxidation increases at higher temperatures.

According to Fig 7, the oxidation of graphite in the air starts at temperatures above 600°C and the rate of oxidation increases at temperatures above 650°C. Considering this fact and based on the combustion temperatures from Table 2, only four mixtures, i.e., mixtures 2, 6, 7 and 8, with maximum temperatures greater than 650°C were chosen to react in the presence of graphite. Not to mention, all conditions for syntheses 2.6.7 and 8 such as, the amount of raw materials, preparing conditions, hot plate temperature, etc. were the same in the presence and absence of graphite.

Considering the oxidation temperature of graphite and ignition temperatures of syntheses reveal that this material plays no role in the synthesis reaction, because the combustion reactions initiate at temperatures much lower than the oxidation temperature of graphite. As a result, the only role taken by graphite in the experiments was to prevent nickel oxidation at high temperatures.

Fig 8 illustrates the XRD patterns for the four selected groups, i.e., those that reacted in the presence of graphite. In all the XRD patterns, nickel in metallic form is recognized as the final synthesis product. Therefore, the additional reduction step is no longer necessary. Synthesis, being the only production step, can keep the specific surface area at the highest possible level. This is because the entire synthesis process from the very beginning, i.e., putting the solution on the hot plate, to the end, i.e., reaching the low temperatures after the synthesis, takes less than 10 minutes.

According to Figs 6 and 8, no evidence of alumina peaks can be detected for the samples where the percentage of alumina and Ni are 10 wt.% and 90 wt.%, respectively. This is attributed to the fact that the high intensity of Ni peaks in the patterns renders alumina peaks unrecognizable. Alumina is synthesized as γ-Al_2O_3 up to 750°C, which has wide and low-intensity peaks while it is crystalline [29]. In contrary with α-Al_2O_3, γ-Al_2O_3 is hard to detect in XRD pattern especially in the presence of metallic elements, not only when its content is 10wt.%, but also till 25wt.% [30,31]. To prove the presence of alumina, the nanocomposite powder (synthesis number 2) was solved in nitric acid (5 M) for 50 h. The solution was kept at 60°C for 2 h while stirring at 160 rpm and for 48 h at room temperature without stirring. The final solution was sent for inductively coupled plasma optical emission spectrometer (ICP-OES) analysis. The results suggested that nickel has a density of 89.6%, which is acceptable considering the nanocomposite stoichiometric (90 wt. % Ni - 10 wt.% Al_2O_3) and different sources of error. In other words, the percentage of alumina is 10 wt. % as expected. Also, Fig 9 and 10 show the XRD pattern and the TEM image taken from agglomerated white alumina powder after solving the nanocomposite in the nitric acid and drying in an oven at 150 °C for 1h. The TEM image shows alumina particles have a

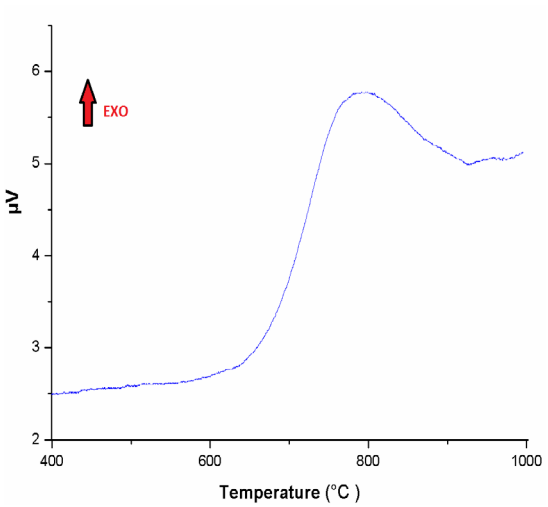

Fig. 7- DSC diagram for graphite oxidation in air.

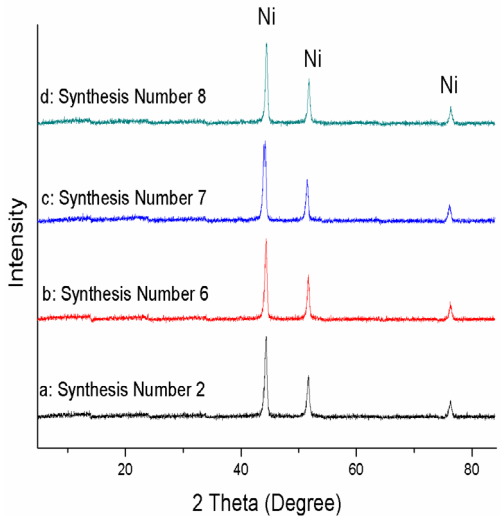

Fig. 8- The XRD results for synthesis in the presence of graphite in the reaction solution.

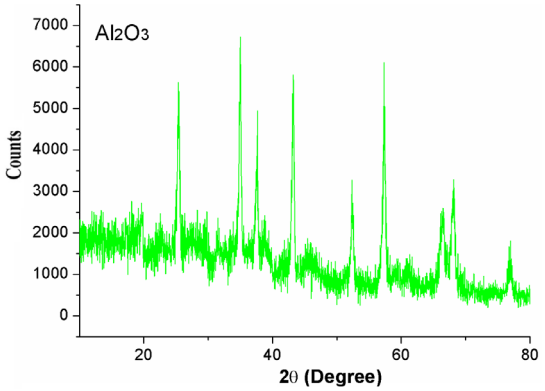

Fig. 9- XRD pattern of alumina after solving metallic nickel in nitric acid.

Fig. 10- TEM image of alumina after solving metallic nickel in nitric acid.

Table 3- BET results for Ni-Al_2O_3 nanocomposites synthesized from different mixtures

synthesis number	2	6	7	8
specific surface area ($m^2 g^{-1}$)	45	38	207	122

mean particle size of less than 25 nm.

Finally, the four nanocomposites synthesized in the presence of graphite were sent for the BET test to measure the specific surface area. The results of BET are given in Table 3.

As shown in Table 3, there are considerable differences in the BET results. Sample number 7 in comparison with numbers 2, 6 and 8 had urea at the lowest level (F/O=1). According to previous papers, urea can decrease the surface area by producing polymeric intermediates, which in turn cause sintering of the synthesized particles during combustion [23]. This means that if the nanocomposite synthesis is done by urea as the only fuel, the surface area is lower. In order to investigate this hypothesis, a BET test was conducted on a Ni–10wt. % Al_2O_3 nanocomposite produced by urea as the sole fuel. The BET result showed that the specific surface area is about 25 m^2g^{-1}. As expected, the amount of specific surface area is lower than other fuels when urea is the only fuel used for synthesis. Glycine and hydrazine could not synthesize nanocomposite successfully when used alone. According to Table 1, glycine cannot reach the critical combustion temperature (600°C) for a crystalline synthesis of the nanocomposite. The nitrate-hydrazine system in contrary to nitrate-urea and nitrate-glycine systems that had visible flame during synthesis, it showed a synthesis without considerable flame and with an explosive voice. The nitrate-hydrazine system had severe sputtering at F/O=1.5. It causes the reaction cannot be completed. Not to mention, syntheses in the presence of a mixture of three fuels occurred with flame and slight sputtering. This justifies the application of a mixture of fuels for achieving a suitable combustion synthesis with high surface area of nanocomposite.

Syntheses 7 and 8 that showed the highest BET results had glycine at F/O=1.5. According to Fig 3 glycine at F/O 1.5 shows an unstable combustion synthesis. So, it can be said, urea and hydrazine play a more important role than glycine on combustion characteristics and amount of surface area. Because it is necessary for a combustion reaction to be completed in the lowest time, what, did not happen in nitrate-glycine system. By referring to Fig 2a and 2c and Table 1 it can be recognized among urea and hydrazine that, hydrazine had rapid decomposition that can cause a rapid combustion reaction. As shown in Table 1, reaction time for urea and hydrazine when F/O=1.5 were 3.1 and 2.9 seconds, respectively. During the reaction periods, hydrazine has a 551°C increase in temperature versus 442°C for urea. In conformity with the findings of other researchers, such a difference suggests a much more vigorous combustion reaction in the presence of hydrazine [32].

The details of the synthesis reaction for the four mixtures are given in Table 4. The region of reaction is the region between ignition and combustion temperatures.

The combustion characteristics in Table 4 show that the highest rate of reaction belongs to synthesis 7 which has the best BET result. It means, released gases during faster combustion

Table 4- Details of the synthesis reaction for samples 2, 6, 7 and 8 from Table 2

synthesis number	ignition temperature (°C)	combustion temperature (°C)	region of reaction (°C)	time of reaction (s)	rate of reaction (°C s^{-1})
2	250	671	421	4.2	100.2
6	185	739	554	5.5	100.7
7	174	726	552	1.7	324.7
8	184	664	480	2.9	165.5

Table 5- Ni crystallite size calculated based on Scherer's method

Synthesis Number	2	6	7	8
Ni Crystallite Size (nm)	17.60	17.58	13.29	15.59

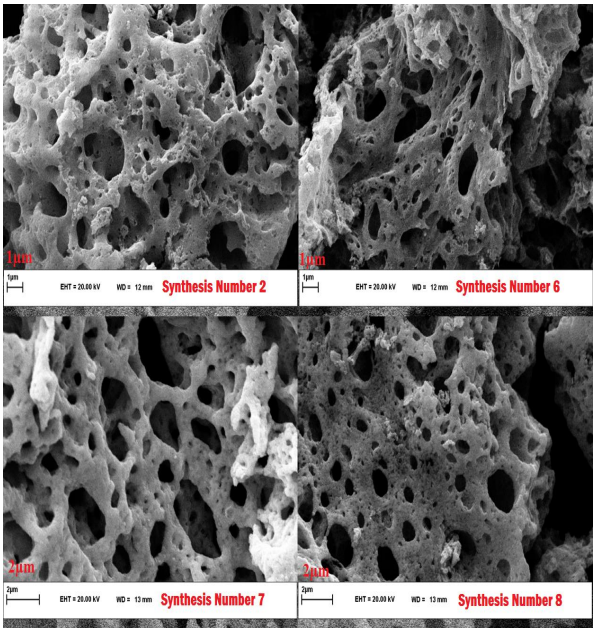

Fig. 11- SEM images of samples number 2, 6, 7 and 8.

reactions increase surface area. Although all gases contribute to heat losses and prevent sintering, the most effective gases for producing porosity and increasing the surface area are those released during the combustion such as N_2 [33]. Hydrazine produces more mol of N_2 in the same conditions as compared to urea and glycine. It releases about 58 mol N_2 in comparison with 44 and 25 mol N_2 for urea and glycine, respectively. Not to mention, even the total mol of gases released by hydrazine (about 277 mol) is more than urea (about 220 mol) and glycine (about 203 mol) in the presence of the same amount of nitrates at F/O=1. Although synthesis number 8 can produce more gases than number 7 (because of a higher amount of fuels), the higher rate of reaction for synthesis 7 can release all gases in less time than synthesis 8 that can have more effect on increasing surface area.

In Table 5, the nickel crystallite sizes are given based on the XRD patterns in Fig 8. The calculation of nickel crystallite size was carried out by Scherer's method [34].

As shown in Table 5, synthesis 7 has the lowest nickel crystallite size. It proves the higher rate of reaction, causes lower crystallite size. SEM and FESEM images of four synthesized nanocomposites are given in Fig 11 and Fig 12.

Fig 11 shows that the all samples are porous even samples with lower BET results. Apparently in images, higher porosity belongs to synthesis 7 that has the highest surface area. In order to better understanding FESEM images are shown in Fig 12.

It can be seen synthesis 7 has small porosities than other syntheses and it causes such high BET results.

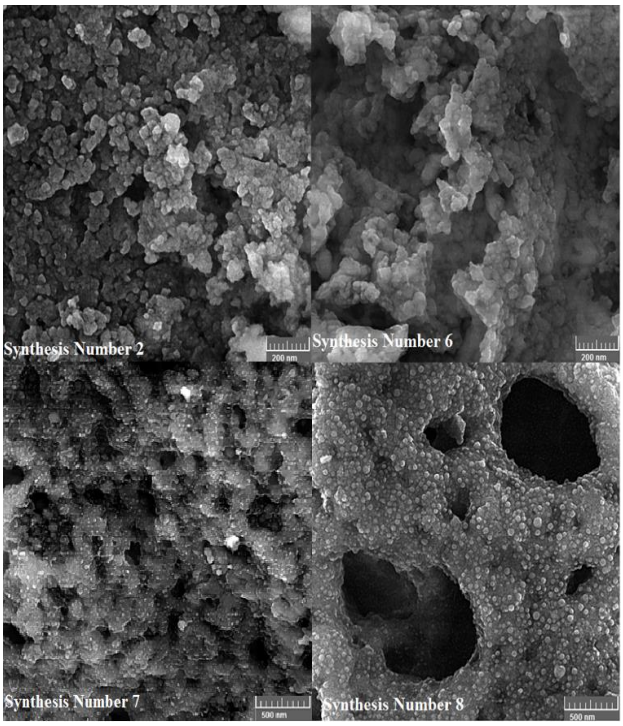

Fig. 12- FESEM images of samples number 2, 6, 7 and 8.

4. Conclusions

This research was devoted to investigating the synthesis of Ni–10wt. %Al_2O_3 nanocomposite by a mixture of three fuels using the SCS method in less than ten minutes in air. The main results and outcomes of this research can be summarized as follows:

Nitrate-hydrazine reaction system has ignition temperature in accordance with hydrazine boiling temperature (110 ˚C).

Excess amount of urea and glycine (F/O >1) in experimental conditions decreases the combustion temperature, from 574 to 443 ˚C.

Synthesized alumina needs temperature more than 600 ºC to synthesize crystalline.

The highest surface area (207 m^2g^{-1}) belongs to the nanocomposite produced with the highest amount of hydrazine and glycine (F/O =1.5) and the lowest amount of urea (F/O= 1).

Faster combustion synthesis causes higher surface area.

Acknowledgments

The authors are grateful to the financial aid from Ferdowsi University of Mashhad, Iran (Grant No. 3/36990).

References

1. Wang H, Han W, Li X, Liu B, Tang H, Li Y. Solution Combustion Synthesis of Cr_2O_3 Nanoparticles and the Catalytic Performance for Dehydrofluorination of 1,1,1,3,3-Pentafluoropropane to 1,3,3,3-Tetrafluoropropene. Molecules (Basel, Switzerland). 2019;24(2):361.

2. Xiao X, Zhang Z, Cai L, Li Y, Yan Z, Wang Y. The excellent catalytic activity for thermal decomposition of ammonium perchlorate using porous CuCo2O4 synthesized by template-free solution combustion method. Journal of Alloys and Compounds. 2019;797:548-57.

3. Khaliullin SM, Zhuravlev VD, Bamburov VG, Khort AA, Roslyakov SI, Trusov GV, Moskovskikh DO. Effect of the residual water content in gels on solution combustion synthesis temperature. Journal of Sol-Gel Science and Technology. 2020 Feb;93(2):251-61.

4. Potanin AY, Vorotilo S, Pogozhev YS, Rupasov SI, Lobova TA, Levashov EA. Influence of mechanical activation of reactive mixtures on the microstructure and properties of SHS-ceramics MoSi2–HfB2–MoB. Ceramics International. 2019;45(16):20354-61.

5. Ortiz-Quiñonez J-L, Pal U, Villanueva MS. Structural, Magnetic, and Catalytic Evaluation of Spinel Co, Ni, and Co-Ni Ferrite Nanoparticles Fabricated by Low-Temperature Solution Combustion Process. ACS Omega. 2018;3(11):14986-5001.

6. Xu C, Manukyan KV, Adams RA, Pol VG, Chen P, Varma A. One-step solution combustion synthesis of CuO/Cu2O/C anode for long cycle life Li-ion batteries. Carbon. 2019;142:51-9.

7. Deganello F, Tyagi AK. Solution combustion synthesis, energy and environment: Best parameters for better materials. Progress in Crystal Growth and Characterization of Materials. 2018;64(2):23-61.

8. Mukasyan AS, Dinka P. Novel approaches to solution-combustion synthesis of nanomaterials. International Journal of Self-Propagating High-Temperature Synthesis. 2007;16(1):23-35.
9. Ianoş R, Păculescu A, Păcurariu C, Lazău I. Solution Combustion Synthesis and Characterization of Magnetite, Fe₃O₄, Nanopowders. Journal of the American Ceramic Society. 2012;95(7):2236-40.
10. González-Cortés SL, Imbert FE. Fundamentals, properties and applications of solid catalysts prepared by solution combustion synthesis (SCS). Applied Catalysis A: General. 2013;452:117-31.
11. Kang W, Ozgur DO, Varma A. Solution Combustion Synthesis of High Surface Area CeO2 Nanopowders for Catalytic Applications: Reaction Mechanism and Properties. ACS Applied Nano Materials. 2018;1(2):675-85.
12. Tarragó DP, Malfatti CdF, de Sousa VC. Influence of fuel on morphology of LSM powders obtained by solution combustion synthesis. Powder Technology. 2015;269:481-7.
13. Vahdat Vasei H, Masoudpanah SM, Adeli M, Aboutalebi MR. Photocatalytic properties of solution combustion synthesized ZnO powders using mixture of CTAB and glycine and citric acid fuels. Advanced Powder Technology. 2019;30(2):284-91.
14. Mirbagheri SA, Masoudpanah SM, Alamolhoda S. Structural and optical properties of ZnAl2O4 powders synthesized by solution combustion method: Effects of mixture of fuels. Optik. 2020;204:164170.
15. Novitskaya E, Kelly JP, Bhaduri S, Graeve OA. A review of solution combustion synthesis: an analysis of parameters controlling powder characteristics. International Materials Reviews. 2021 Apr 3;66(3):188-214.
16. Yilmaz E, Sonmez MS. The influence of process parameters on the chemical and structural properties of solution combustion prepared vanadium pentoxide. Materials Letters. 2020;261:127095.
17. Li P, Hu X, Zhang Z, Wen M, Chen M, Yu B, et al. A series of Ni–Al2O3 catalysts derived from layered double hydroxides for vapor phase catalytic exchange between water and hydrogen. International Journal of Hydrogen Energy. 2021;46(63):32036-43.
18. Muangnapoh T, Srimara P, Vas-Umnuay P. Template- and Magnetic Field-Free Chemical Reduction of Ni Nanochains for Ni-Al(2)O(3) Cermet Films: Growth Control, Characterization, and Application. ACS Omega. 2020;5(38):24584-91.
19. Serdyukov SI, Kniazeva MI, Sizova IA, Zubavichus YV, Dorovatovskii PV, Maximov AL. A new precursor for synthesis of nickel-tungsten sulfide aromatic hydrogenation catalyst. Molecular Catalysis. 2021;502:111357.
20. Cui C, Liu Y, Mehdi S, Wen H, Zhou B, Li J, et al. Enhancing effect of Fe-doping on the activity of nano Ni catalyst towards hydrogen evolution from NH3BH3. Applied Catalysis B: Environmental. 2020;265:118612.
21. Patil KC, Aruna ST, Mimani T. Combustion synthesis: an update. Current Opinion in Solid State and Materials Science. 2002;6(6):507-12.
22. Mekasuwandumrong O, Wongwaranon N, Panpranot J, Praserthdam P. Effect of Ni-modified α-Al2O3 prepared by sol–gel and solvothermal methods on the characteristics and catalytic properties of Pd/α-Al2O3 catalysts. Materials Chemistry and Physics. 2008;111(2-3):431-7.
23. Tahmasebi K, Paydar MH. The effect of starch addition on solution combustion synthesis of Al2O3–ZrO2 nanocomposite powder using urea as fuel. Materials Chemistry and Physics. 2008;109(1):156-63.
24. Deshpande K, Mukasyan A, Varma A. Direct Synthesis of Iron Oxide Nanopowders by the Combustion Approach: Reaction Mechanism and Properties. Chemistry of Materials. 2004;16(24):4896-904.
25. Avgouropoulos G, Ioannides T. Selective CO oxidation over CuO-CeO2 catalysts prepared via the urea–nitrate combustion method. Applied Catalysis A: General. 2003;244(1):155-67.
26. Stewardson D. Design and Analysis of Experiments Design and Analysis of Experiments 5hEd by Douglas C Montgomery 2001 , John Wiley , New York . Hard-Bound, 684 pp ISBN 0 471 31649 0. MSOR Connections. 2001;1(1):15-6.
27. Liu Y, Qin M-l, Zhang L, Jia B-r, Cao Z-q, Zhang D-z, et al. Solution combustion synthesis of Ni–Y2O3 nanocomposite powder. Transactions of Nonferrous Metals Society of China. 2015;25(1):129-36.
28. D.R. Gaskell., Introduction to the Thermodynamics of Materials, 4th ed, Tylor and Francis Books, 2003.
29. Samain L, Jaworski A, Edén M, Ladd DM, Seo D-K, Javier Garcia-Garcia F, et al. Structural analysis of highly porous γ-Al2O3. Journal of Solid State Chemistry. 2014;217:1-8.
30. Nasiri H, Bahrami Motlagh E, Vahdati Khaki J, Zebarjad SM. Role of fuel/oxidizer ratio on the synthesis conditions of Cu–Al2O3 nanocomposite prepared through solution combustion synthesis. Materials Research Bulletin. 2012;47(11):3676-80.
31. Yalamaç E, Trapani A, Akkurt S. Sintering and microstructural investigation of gamma–alpha alumina powders. Engineering Science and Technology, an International Journal. 2014;17(1):2-7.
32. GarcÍa R, Hirata GA, McKittrick J. New combustion synthesis technique for the production of (InxGa1−x)2O3 powders: Hydrazine/metal nitrate method. Journal of Materials Research. 2001;16(4):1059-65.
33. Patil KC, Hegde MS, Rattan T, Aruna ST. Chemistry of Nanocrystalline Oxide Materials: WORLD SCIENTIFIC; 2008 2008/09.
34. Shehata F, Fathy A, Abdelhameed M, Moustafa SF. Preparation and properties of Al2O3 nanoparticle reinforced copper matrix composites by in situ processing. Materials & Design. 2009;30(7):2756-62.